Lab on a Chip

Accepted Manuscript

ROYAL SOCIETY OF CHEMISTRY

www.rsc.org/loc

Modeling and Optimization of Acoustofluidic Micro-Devices†

Philipp Hahn*, Olivier Schwab and Jurg Dual

Received Xth XXXXXXXXXX 20XX, Accepted Xth XXXXXXXXX 20XX
First published on the web Xth XXXXXXXXXX 200X
DOI: 10.1039/b000000x

We investigate how the combination of numerical simulation tools and optimization routines can be used to design micro-devices. Experimental devices that are designed in this way can only provide optimal performance if the simulation model, used in the optimization procedure, reflects the real device characteristics accurately. Owing to this fact, the modeling of acoustofluidic devices is summarized. The mathematical formulation of the optimization problem, the parameterization of the device design and the implementation of the optimization loop is addressed alongside with practical recommendations for the chosen genetic algorithm optimization. In order to validate the implementation, an optimized planar resonator is compared with the optimal geometry given in the literature. The optimization of a typical 3D micro-device shows that devices can be designed to generate any desired acoustic mode shape at maximum pressure amplitude. The presented automatic design approach is of great practical relevance for the development of highly optimized micro-devices and it can speed up and facilitate the design-process in the growing field of acoustofluidics.

1 Introduction

Ultrasonic standing waves within the fluid cavity of a particle manipulation device can be generated via piezoelectric excitation. Acoustic radiation forces, caused by the nonlinear interaction between the time-harmonic acoustic field and a particle can be used to manipulate particles in suspension. This allows for contactless handling of cells, bacteria or other particles, suggesting a wide range of lab-on-a-chip applications in the life sciences. A comprehensive review of theoretical work, experimental setups as well as recent developments can be found in the acoustofluidics tutorial series.[1]

Due to the growing performance of computing hardware and the increasing user-friendliness of simulation software, the numerical modeling of even complex 3D acoustofluidic devices has become feasible and time-efficient. For this reason, numerical simulations are an important tool for the design of new experimental particle manipulation setups.

To date, the typical design procedure relies on iterative manual adjustments and parameter studies of the numerical model. Starting with an initial model geometry and structure, the simulation results are used to evaluate the shape and amplitude of the Gor'kov potential. Assuming that viscous effects can be neglected, this potential defines the acoustic radiation forces on small spherical particles inside the acoustic field.[2,3] Subsequently, the model geometry is altered until the desired Gor'kov potential is obtained. Unfortunately, this iterative design process is time-consuming and requires physical intuition.

In order to differentiate systematically between different design levels, the concepts of topology, shape, and sizing are employed in this paper.[4] Clearly, the choice of a suitable device topology is a fundamental step which is hard to automate since it requires engineering know-how. However, once the topology of a simulation model is chosen, finding the optimal shape and sizing of the device components is well suited for automation because this can be parametrized easily. One example is the design of a particle trap.[5] In this case, the shape of the channel walls could be parametrized and changed until optimal trapping performance is predicted by the numerical simulation. Another example is the design of a planar resonator.[6] Representing a pure sizing problem, the thickness of the individual device layers could be changed until the desired force field in the fluid layer is attained.

The most straightforward way to solve such optimization problems is a parameter study where the chosen parameters are changed stepwise within the relevant parameter range. However, if the parameter space becomes large, *i.e.* the number of relevant parameters and the number of steps is large, the number of parameter combinations, each related to a separate device simulation, grows extremely fast. If, for example, there are five parameters which are iterated in 20 steps, a total of 20^5 simulations are required to search the parameter space for the optimal solution. Assuming one simulation run takes 30 s, the device optimization would take more than three years. In order to reduce the computational ef-

Institute of Mechanical Systems (IMES), Department of Mechanical and Process Engineering, ETH Zurich, Tannenstrasse 3, CH-8092 Zurich, Switzerland. Tel: +41 44 633 9237; E-mail: hahnp@ethz.ch

† Electronic Supplementary Information (ESI) available: [Matlab code for the optimization of a planar resonator and a 3D micro-device as well as the FE models]. See DOI: 10.1039/b000000x/

fort, more sophisticated optimization methods have been developed that make use of trends in the objective function which quantifies how good the result, corresponding to a specific parameter combination is.[7,8] Deterministic methods, called mathematical programming, use information on the local gradient of the objective function to achieve fast convergence towards the optimum. However, these methods usually converge to a local optimum if the objective function is non-convex.[9] Real-world optimization problems often have a large number of local optima and therefore require stochastic approaches to find the globally best parameter combination.[10] Among others, genetic algorithms (GA), simulated annealing and particle swarm optimization are frequently used. In the present work, we choose GA since they have been applied successfully to many similar optimization problems as reported in the literature.[11,12]

When using an optimization-based design approach, it has to be understood that the optimization result can only be as good as the numerical model. To emphasize this fact, the modeling of acoustofluidic micro-devices is briefly reviewed. Subsequently, the optimization problem for acoustofluidic devices is formulated for the solution by GA. Specifics on the numerical implementation are provided and the optimization of two devices is detailed. The planar resonator serves as a proof of concept for the proposed optimization approach. Finally, the optimal design of a silicon micro-device is shown, comprising all aspects of a real-life device design problem.

2 Modeling of acoustofluidic Devices

The main goal of numerical modeling in the context of acoustophoresis is to predict the motion of particles inside fluid cavities or channels. The relevant physics is governed by the Navier-Stokes equation for the fluid,[13] the elastodynamic equations for all solid parts of the device[14] and electromechanical coupling at the piezoelectric transducer.[15] At the interfaces between the fluid and the solid domains, fluid-structure interaction takes place.

2.1 The Basic Device Model

Even though the piezoelectric excitation is purely time-harmonic, the nonlinear terms in the Navier-Stokes equations give rise to time-averaged forces on particles in fluid suspension. Due to the amplitude scale difference between the time-harmonic and the time-averaged fields, the problem can be studied in good approximation by a perturbation expansion for the field variables in the Navier-Stokes equations.[3,16] This approach has the advantage that numerical problems related to the time scale difference between the ultrasonic cycle and the transients as well as the amplitude scale difference between the first-order time-harmonic and the second-order time-averaged fields can be circumvented.

If water is used in an experimental setup, as often the case, the viscous effects on the velocity field can be neglected in the bulk part of the ultrasonic field. Under this assumption, the first-order stress and velocity fields inside the fluid are governed by the acoustic wave equation which, for time harmonic fields, reduces to a Helmholtz equation. Hence, the first-order field can be obtained by a frequency domain analysis of the coupled elastodynamic, piezoelectric and Helmholtz equations. All time-harmonic fields $A(\boldsymbol{r},t)$ can be written in the form,

$$A(\boldsymbol{r},t) = \mathrm{Re}\left[A(\boldsymbol{r})\mathrm{e}^{\mathrm{i}\omega t}\right], \tag{1}$$

with the angular frequency ω, time t and the complex-valued magnitude $A(\boldsymbol{r})$ as a function of the position vector $\boldsymbol{r}$. It is understood that the following differential equations describe the magnitude of field variables corresponding to $A(\boldsymbol{r})$, whereas the position dependence is omitted from here on. The displacement field u_i in the structural parts of the device is related to the stress field σ_{ij} according to the dynamic equilibrium,

$$\sigma_{ij,j} + \rho\omega^2 u_i = 0. \tag{2}$$

The material density is ρ and it is noted that all differential equations in this paper are written in index notation to the orthonormal basis x_i; $i = 1,2,3$ whereas $_{,i}$ indicates a derivative with respect to x_i. Further, the kinematic relations translate the displacement field into the strain field γ_{ij},

$$\gamma_{ij} = \frac{1}{2}\left(u_{i,j} + u_{j,i}\right), \tag{3}$$

and the constitutive law expresses the stress field as a function of the strain field $\sigma_\lambda = \sigma_\lambda(\gamma_\mu)$, whereas piezoelectric materials show an additional dependence on the electric field E_k according to $\sigma_\lambda = \sigma_\lambda(\gamma_\mu, E_k)$. Greek indices are interpreted as double indices[15] and both constitutive laws are discussed in section 2.3. As explained above, the first-order pressure field p in the bulk of the fluid follows the Helmholtz equation,

$$p_{,ii} = -k^2 p, \tag{4}$$

with the wavenumber $k = \frac{\omega}{c}$ as a function of the speed of sound c in the fluid. The first-order velocity field v_i is calculated by

$$v_i = \mathrm{i}\frac{1}{\rho_0\omega}p_{,i}, \tag{5}$$

with the quiescent fluid density ρ_0. Inviscid fluid-structure interaction is implemented by velocity continuity in interface normal direction n_i,

$$\mathrm{i}\omega u_i n_i = v_i n_i, \tag{6}$$

continuity of the traction vector in the normal direction,

$$\sigma_{ij} n_j = -p n_j, \tag{7}$$

and zero traction in two different tangential directions t_j,

$$\sigma_{ij} t_j = 0. \tag{8}$$

The calculated time-harmonic first-order solution enters the second-order time-averaged equations as a source term and causes the acoustic radiation force on all objects distorting the first-order field inside the fluid. The radiation force can be deduced from the undisturbed first-order field by analytical expressions that are based on scattering theory.[3] Solutions exist for a number of simple particle shapes, the most relevant one being for elastic spheres with a radius much smaller than the acoustic wavelength since particles of this type are used in many experiments. The original derivation was carried out by Gor'kov,[2] who formulates the radiation force F_i^{rad} as the negative gradient of the so-called Gor'kov potential U,

$$F_i^{\mathrm{rad}} = -U_{,i}, \tag{9a}$$

where U is a function of the first-order field and the particle-fluid combination according to

$$U = \frac{4\pi}{3}a^3\left[f_1\frac{1}{2}\kappa_0\left\langle p(\boldsymbol{r},t)^2\right\rangle - f_2\frac{3}{4}\rho_0\left\langle v_i(\boldsymbol{r},t)^2\right\rangle\right], \tag{9b}$$

$$f_1 = 1-\tilde{\kappa},\ \text{with}\ \tilde{\kappa} = \frac{\kappa_p}{\kappa_0}, \tag{9c}$$

$$f_2 = \frac{2(\tilde{\rho}-1)}{2\tilde{\rho}+1},\ \text{with}\ \tilde{\rho} = \frac{\rho_p}{\rho_0}. \tag{9d}$$

The time-average of the time-harmonic field variables can be calculated as $\left\langle p(\boldsymbol{r},t)^2\right\rangle = \frac{1}{2}\left(pp^*\right)$ and $\left\langle v_i(\boldsymbol{r},t)^2\right\rangle = \frac{1}{2}\left(v_i v_i^*\right)$, where the asterisk denotes complex conjugation. The particle radius is a and the monopole coefficient f_1 depends on the particle compressibility $\kappa_p = \frac{1}{K}$ for a solid particle with the bulk modulus K and fluid compressibility $\kappa_0 = \frac{1}{\rho_0 c_0^2}$ with c_0 specified below in eqn (10). The dipole coefficient f_2 depends only on the particle and fluid density ρ_p and ρ_0, respectively. A formulation that additionally takes into account the viscous boundary layer surrounding the spherical particle is derived by Settnes and Bruus,[17] including the conditions under which this viscous correction becomes relevant. Balancing the calculated radiation force plus the buoyancy force with the well-known Stokes drag on a sphere directly leads to the particle-fluid relative velocity because inertial effects can typically be neglected.[18] If no analytical expression for the radiation force is available, it can be obtained from a numerical simulation of the scattering field around the particle.[19,20] Nevertheless, simulating the trajectory of complex shaped particles also requires a hydrodynamic model that is more involved.[21]

2.2 Advanced Modeling and Acoustic Streaming

Particularly challenging to model are conditions in which particles are in close proximity to each other or to the cavity walls. In these situations the scattering field of the particles leads to the so-called secondary acoustic radiation force.[22] The viscous boundary layer on the surface of particles or walls can also become important in this case. Under these conditions, both irrotational and solenoidal parts of the first-order field need to be taken into account.[19] However, the secondary acoustic radiation force is often small in comparison with the primary radiation force and it decreases very fast as the particle-particle or the particle-wall distance increases. Nevertheless, the magnitudes of the secondary and primary acoustic radiation force need to be compared in order to decide if the secondary force needs to be taken into account under the specific experimental conditions. Certainly, the secondary forces become relevant if the particle concentration is extremely high or if one is interested in the final particle configuration when many particles collect at the same location. The simulation of particle traces under these conditions is also challenging from a hydrodynamic point of view since the hydrodynamic drag force is affected by the presence of other particles or cavity walls.[23]

Besides the acoustic radiation force there exists a second time-averaged effect called acoustic streaming.[24,25] Similar to the radiation forces, this bulk fluid motion can also be identified as a second-order time-averaged effect driven by the first-order field. However, the viscous boundary layers in the first-order field play an essential role here since they are the main driving mechanism for the acoustic streaming in mm-sized or sub mm-sized fluid cavities. Streaming provides another means of manipulating micro-particles by the hydrodynamic drag forces between particles and the fluid.[26] The radiation forces exhibit cubic scaling with the particle radius, whereas the streaming drag forces on a fixed particle scale only linearly with the latter. Depending on the particle-fluid combination, the resonance mode and the geometry of the fluid cavity, the different scaling gives rise to a transition from radiation force domination to acoustic streaming domination as the particle size is decreased.[27] For any given experimental conditions, it needs to be assessed if acoustic streaming considerably affects the particle motion. This step is not straight forward because the geometry of the fluid cavity and the resonance mode affect the critical particle radius at which the transition appears. Muller et al. provide a good estimate of the critical particle radius.[28] Particle materials of low acoustic contrast lead to a larger critical radius than materials of high acoustic contrast. Also, it should be considered that the locations of zero radiation force are solely affected by streaming. From a numerical point of view, acoustic streaming is still an active field of research because the resolution of the thin acoustic boundary layers in a fluid cavity is computationally very demanding but there are ways to avoid this problem.[29,30]

2.3 Material Properties and Loss Mechanisms

In addition to the fluid-particle suspension, acoustofluidic micro-devices are typically composed of materials like piezoelectric ceramics, silicon, glass, metal, and polymers

in the form of glue layers. As observed in the equations above, the response of these materials on ultrasonic excitation depends on their elastic properties, *i.e.* the speed of sound or the constitutive law. Special care is required in the device modeling since some of the materials listed above exhibit anisotropic behavior and show significant frequency and temperature dependence.

Device resonances are subject to a number of loss mechanisms that limit the amplitudes and widen the frequency bandwidth.[19] The losses can be modeled by a complex speed of sound for fluids and a complex constitutive law for solids.[31,32] This loss model is valid for harmonic fields under the assumption of low damping and leads to the complex speed of sound and wavenumber,

$$c \approx c_0 \left(1 + \mathrm{i}\frac{\varphi}{2}\right) \text{ and } k \approx k_0 \left(1 - \mathrm{i}\frac{\varphi}{2}\right), \tag{10}$$

as a function of the dimensionless loss factor φ, containing all relevant dissipation effects in the fluid. It is not straightforward to predict the loss factor since it depends not only on the material, the temperature and the frequency but it is also very sensitive on the geometry of the fluidic cavity and the resonance mode. The reason is the viscous boundary layer at the fluid structure interfaces which, in the context of acoustofluidic micro-devices, is a major source of damping in water.[31,33] Only taking into account the viscous damping in the bulk of the fluid leads to an over-estimation of the acoustic amplitudes and radiation forces, especially for fluid cavities in the microscale. It is also worth noting that the speed of sound in water is sensitive on temperature.[34]

The general constitutive law for a lossy linear elastic material can be written as

$$\sigma_{ij} = c_{ijkl}\gamma_{kl}, \tag{11}$$

where the forth order stiffness tensor c_{ijkl} is further split up according to

$$c_{ijkl} = c'_{ijkl} + \mathrm{i}c''_{ijkl}, \tag{12}$$

into the storage and the loss tensors c'_{ijkl} and c''_{ijkl}, respectively.[35] For isotropic materials, the stiffness tensor depends only on the two Lamé parameters λ and μ, reducing the constitutive law to

$$\sigma_{ij} = \lambda\gamma_{kk}\delta_{ij} + 2\mu\gamma_{ij}. \tag{13}$$

This is possible because of the symmetry properties of the stiffness tensor.[14,36] Analog to eqn (12), the Lamé parameters are split up into storage parameters (λ', μ') and loss parameters (λ'', μ''),

$$\lambda = \lambda' + \mathrm{i}\lambda'' \text{ and } \mu = \mu' + \mathrm{i}\mu''. \tag{14}$$

In the context of particle manipulation devices, materials like steel, aluminum, glass, and most polymers are usually modeled as being isotropic. The storage and loss parameters can be measured experimentally or they can be found in the literature.[34,37] Unfortunately, most references only provide a single loss parameter which is related to the propagation of dilatational waves. However, the dissipation in low-loss materials like steel, aluminum or silicon is typically negligible in comparison to other loss mechanisms. For these materials, λ'' and μ'' can be neglected in the device model. The loss parameters for highly dissipative device components like polymer parts or glue layers can be obtained from literature or measurements. Regarding the constitutive law of monocrystalline silicon and its temperature dependence, the reader is referred to the literature.[38,39]

From the linear constitutive equations of piezoelectric materials in stress-charge form,

$$\sigma_\lambda = c^E_{\lambda\mu}\gamma_\mu - e_{k\lambda}E_k, \tag{15a}$$

$$D_i = e_{i\mu}\sigma_\mu + \varepsilon^S_{ik}E_k \tag{15b}$$

it becomes evident that the electric field E_k and the electric displacement field D_i are coupled to the mechanical fields. The mechanical stiffness at constant electric field is denoted as $c^E_{\lambda\mu}$, the permittivity at constant strain is ε^S_{ik}, and $e_{k\lambda}$ is the stress piezoelectric coefficient. Values for the material parameters in eqn (15a) and (15b) are usually provided by the manufacturer.[40] Similar as above, mechanical, piezoelectric, and dielectric damping can be implemented via complex stiffness, permittivity, and stress piezoelectric coefficient tensors.[41,42] The losses show a complex dependence on the driving conditions and the vibration mode, which makes an accurate modeling difficult. Usually, only the dielectric loss factor and the mechanical quality factor for one or two fundamental modes are provided by the manufacturer.[40]

Additional to the damping in the device materials, there are loss mechanisms related to surface and the support of the device.[39,43] Losses into the surrounding air can be neglected if the device is not extremely small or thin but the so-called anchor loss can play an important role. This loss is related to the radiation of waves into the device support or tubes that are necessary for the fluid supply of flow-through devices. Anchor loss is frequency dependent since the energy transfer varies with the vibration mode. Generally speaking, it can be minimized by having a big acoustic impedance difference between the device and adjacent parts. However, due to the common material choice, a soft and light support can be realized more easily than a stiff support. A simple solution is to place the device on a base made of foam or tissue paper. In this way, the anchor loss into the support can often be neglected. Modeling a relatively dense or stiff device support or connection tube is more involved. Contact pairs (*e.g.* the device and its support) which are not bonded or sufficiently clamped to each other might have a unilateral or non-uniform contact. This cannot be modeled easily in a frequency domain simulation. An accurate treatment of radiation loss into well bonded parts (*e.g.*

tubes that are glued to the device) requires the use of perfectly matched layers (PML) in the finite element (FE) simulation.[44,45] Since the wavelengths in the device and in the bounding structure can differ by orders of magnitudes, this approach comes with the drawback of a high computational effort due to fine discretization.

2.4 Remarks on the Numerical Implementation

If all fields vary only in one dimension, the differential equations above can be cast into the framework of the transmission line approach, the transfer matrix model or electro-acoustic equivalent circuits.[6,46] These 1D models are numerically efficient but they can only be applied to layered resonators with negligible lateral effects. In the course of miniaturization for lab-on-a-chip applications, the device dimensions become comparable in all directions and the geometry is often complex. These devices require more sophisticated 2D and 3D numerical models. From the variety of numerical methods for the solution of differential equations, the finite element method (FEM) is often chosen for its flexibility and because of readily available commercial implementations that support the coupling for multiphysics simulations. The numerical discretization into mesh elements and the element order affect the accuracy of the simulation.[47] Care must be taken in order to assure that all fields and geometric features are resolved sufficiently. In this context, convergence studies with increasing mesh sizes are often helpful to define a suitable meshing setting. Even though glue layers might be extremely thin, they still affect the device vibration significantly because the glue stiffness is low in comparison to other device materials and the dissipation is high. However, the representation of thin glue layers or thin cover slides is a challenge in a numerical simulation because the number of elements in the FE mesh quickly becomes too large. This problem can be solved by using thin layer approximations for the glue and plate or shell elements for thin cover slides.

3 Device Design by Genetic Algorithm Optimization

With the goal of an automated device design setup in mind, the effects of secondary radiation forces and acoustic streaming, as outlined in section 2, only need to be incorporated in the numerical model if they are essential for the device performance. Clearly, this is problem dependent and the important effects need to be picked from paragraphs above. In this section, we primarily want to study the potential of the numerical optimization of acoustofluidic devices. Therefore, we focus on the basic device model as outlined in section 2.1 in order to keep it simple. However, it is emphasized that in future device optimization studies, the model can be more complex and e.g. also include streaming effects. In summary, from here on we consider particles which are accurately described by the Gor'kov theory, neglecting the viscous correction to the radiation force as well as particle-particle and particle-wall interaction. Furthermore, we assume that the device is operating in a radiation force dominated regime and do not incorporate acoustic streaming in the model. Despite its simplicity, the chosen model covers a large spectrum of experimental setups. Acoustophoresis is often used to manipulate many particles at a time, meaning that the focus is on the bulk particle motion rather than on single particle trajectories which might be affected by secondary radiation forces. Small quantitative deviations in the predicted particle velocities due to the viscous correction of the radiation force are also less crucial in this context.

In an optimization problem, the objective function $f(\boldsymbol{p})$ quantifies the device performance based on the simulation result for the parameter vector $\boldsymbol{p}$. Conventionally, the optimization problem is formulated in a way that a small value relates to a good performance,[8]

$$\begin{aligned} &\text{minimize } f(\boldsymbol{p}) \\ &\quad \text{with } \boldsymbol{g}(\boldsymbol{p}) \leq \boldsymbol{0},\ \boldsymbol{h}(\boldsymbol{p}) = \boldsymbol{0} \\ &\quad \text{and } \boldsymbol{p}_\mathrm{l} \leq \boldsymbol{p} \leq \boldsymbol{p}_\mathrm{u}. \end{aligned} \tag{16}$$

The inequality conditions $\boldsymbol{g}(\boldsymbol{p}) \leq \boldsymbol{0}$ and the equality conditions $\boldsymbol{h}(\boldsymbol{p}) = \boldsymbol{0}$ enforce geometric constraints due to the device design, whereas the range of feasible parameter values is prescribed by a lower bound $\boldsymbol{p}_\mathrm{l}$ and an upper bound $\boldsymbol{p}_\mathrm{u}$.

3.1 Implementation

For the numerical solution of the optimization problem, the optimization loop depicted in Fig. 1 is implemented. The initial population consists of random parameter combinations within the feasible parameter range. The optimization loop is terminated as soon as a certain stop criterion is met, whereas we stop it manually. In our

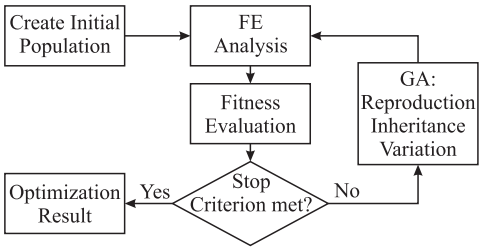

Fig. 1 Flowchart of the numerical genetic algorithm (GA) optimization loop. After the finite element (FE) analysis of all parameter combinations in one generation, there is a fitness evaluation based on the objective function. The population of individuals (*i.e.* parameter combinations) is modified by the GA until a satisfactory solution is found. The GA uses reproduction, inheritance, and variation to create a new population of individual parameter combinations.

implementation, Matlab provides the framework for the routine because it comes with a ready-to-use genetic algorithm implementation as part of the global optimization toolbox and it simplifies the code development as well as the data analysis. The FE analysis of the model is performed in Comsol Multiphysics (version 4.3a) which can be coupled with Matlab via Comsol LiveLink. In this way, the parameter vector can be transmitted from Matlab to Comsol Multiphysics and the simulation results can be read back for the subsequent fitness evaluation. Unforeseen problems in the FE analysis can appear from time to time *e.g.* due to meshing errors for unfavorable parameter combinations. Since many hundreds or thousands of simulations need to be run during one optimization, the probability is high that at least one problem arises. To avoid crashing of the optimization routine, an error handling routine is implemented. The numerical efficiency of the optimization procedure can be improved if multiple FE simulations, each corresponding to one parameter combination, are invoked in parallel. For this reason, a parallel version of the optimization code is used.

3.2 Parametrization of the Device

As mentioned in the introduction, it is reasonable to prescribe the topology of the device and only change the dimensions or, in some cases, the shape of individual device components. In this way, manufacturability can be ensured and over-complex designs are avoided. The key-question in the parametrization of the device design is which attributes to choose. The more parameters, the more flexibility the optimization has to develop a good design. On the other hand, the more parameters, the higher the necessary computing time to search the parameter space for the optimal solution. The computing time increases with the size of the parameter space. For this reason, all efforts must be made to keep the number of parameters (equal to the dimensionality of the parameter space) and the parameter ranges as small as possible. It is one of the main engineering tasks in this automated design process to identify the parameters which are important for the device performance and to choose proper parameter ranges. In addition to the geometric aspects, it is often reasonable to choose the excitation frequency of the transducer as an additional parameter. If the dimensions of the transducer are prescribed, the optimization can still leverage transducer resonances in this way.

3.3 Objective Function

One of the most important steps in the optimization procedure is the fitness evaluation based on the objective function since it defines which device design will be considered optimal. Depending on the task of the device, different objective functions are conceivable. For a 1D planar resonator working at the half wavelength mode for example, it might be sufficient to evaluate only the maximum force on the particles since the shape of the pressure field is prescribed by the range of feasible fluid layer thicknesses. Devices for sensor applications, on the other hand, suggest an objective function based on the radiation force towards or away from the sensor surface.[6] For more complex devices with acoustic fields varying in two or three dimensions, we recommend a formulation based on the Gor'kov potential since it contains all information necessary to obtain the desired particle motion. The objective function,

$$f(\boldsymbol{p}) := -\frac{1}{V}\int_V U(\boldsymbol{p})\hat{U}\mathrm{d}V, \tag{17}$$

is essentially a linear integral transform with the kernel $\hat{U}$ and it evaluates both, shape and magnitude of the simulated force potential $U(\boldsymbol{p})$. The integration is performed over the relevant fluid volume V and it is normalized with the latter to avoid a volume dependence. The kernel is chosen to be the desired normalized force potential. In this way, the objective function becomes minimal for a $U(\boldsymbol{p})$ of high magnitude and of similar shape as $\hat{U}$. For 2D problems, the integration is 2D and the normalization is done with the integration surface. In order to calculate the objective function value $f(\boldsymbol{p})$ for a specific parameter vector $\boldsymbol{p}$, the simulated pressure and velocity fields are exported from the FE analysis and inserted in eqn (9a)-(9d). This provides $U(\boldsymbol{p})$ which subsequently can be plugged into eqn (17). An objective function based directly on the radiation force, as defined in eqn (9a), might be advantageous in some cases but it is not tested here because eqn (17) led to good optimization results.

3.4 Genetic Algorithm

In this work, the optimization problem eqn (16) is solved by the GA. They are based on the ideas of reproduction, inheritance, variation, and selection which are borrowed from evolutionary biology.[10] A population of individuals is initialized and altered by the above mechanisms over multiple generations. Each individual represents a set of parameters, defining the design of the device. In this sense, the parameters are equivalent to genes and the optimization is equivalent to evolution. Each generation, a new population is created, following a set of adjustable rules.[9] The crossover ratio specifies which fraction of new parameter combinations, or children, are created through recombination of current parameter vectors, or parents. The individuals that led to the best simulation results are kept in the population, whereas their number is defined by the elite count. The rest of the children is created through mutation of current individuals. A large number of test optimizations with 2D and 3D device models has been run in order to provide recommendations for a setting which robustly leads to good results. The parents for crossover and mutation are selected by stochastic uniform sampling based on a rank scaling of the current population. The crossover of two parents into a child is governed

by the combination of parameters, each picked from one of the parents in a random fashion. The mutation function, called adaptive feasible, randomly changes the parameter vector and ensures that the constraints are still satisfied. Two elite individuals are kept in the population and all termination conditions are turned off. Regarding the population size and the crossover fraction, only a relative recommendation can be given since they both have a similar effect and the best choice depends on the optimization problem. The larger the number of local optima in the parameter space, the more stochastic search is needed for a global optimization. This can be achieved by choosing a large population or a small crossover ratio since both settings strongly affect the balance between stochastic and directed search. Each of the local optima in the objective function corresponds to a resonance with enhanced radiation forces. The number of these resonances increases with the complexity of the device and scale with the size of the parameter space. Therefore, the optimization of a complex 3D device model over a large parameter space requires a larger population or less crossover than *e.g.* the optimization of a planar resonator over a small parameter space. Another effect which can be observed in the Matlab implementation is that parameters of high magnitude have a stronger influence on the optimization than other parameters. Therefore, normalization of the individual parameters is recommended but the effect can also be used to weight the importance of different parameters.

4 Optimization Results

In this section, two acoustofluidic devices are optimized to provide a proof of concept and to demonstrate the practical relevance of the developed optimization setup. All Matlab files and the FE models are provided as electronic supplementary information.† The computations are performed on a regular PC equipped with a quad-core Intel i7-2600K CPU, 32 GB RAM (DDR-3 1600 MHz) and Windows 7 (64-bit).

4.1 Optimization of a Planar Resonator

The planar resonator has been investigated thoroughly in the literature.[6,46] It is the only acoustofluidic device, for which a well documented optimization has been published. Glynne-Jones et al.[6] use a transfer impedance model for the individual resonator layers and the KLM model for the piezoelectric excitation. Their optimal configuration is used here as a reference to analyze the presented optimization setup. As shown in Fig. 2, the layers of the planar resonator appear in the order: piezoelectric element, carrier layer, fluid, and reflector with thicknesses l_p, l_c, l_f, l_r, respectively. The thickness of the piezoelectric element is always kept constant at $l_\mathrm{p} = 1\,\mathrm{mm}$ whereas the other thicknesses and the excitation frequency f are

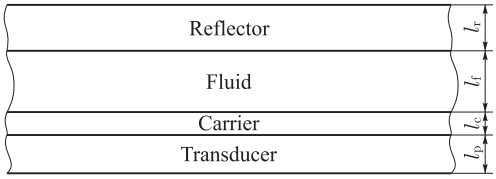

Fig. 2 Layered structure of a planar resonator with the layer thicknesses indicated. It can be analyzed in 1D since the lateral dimensions are much larger than the thickness.

the optimization parameters. The reflector and the carrier layer made of glass are modeled as acoustic domains with $c_0 = 6000\,\mathrm{m/s}$ and $\rho_0 = 2240\,\mathrm{kg/m^3}$. Also modeled as acoustic domain is the water with $c_0 = 1480\,\mathrm{m/s}$ and $\rho_0 = 1000\,\mathrm{kg/m^3}$. Both materials are implemented with a loss factor of $\varphi = 0.01$ to account for all losses. The piezoelectric material used by Glynne-Jones et al. is called PZT4D and modeled with the following parameters of the KLM model[42] for a thickness resonance: speed of sound $c = 4530(1 + \mathrm{i}/(2Q_\mathrm{m}))\,\mathrm{m/s}$, mechanical quality factor $Q_\mathrm{m} = 100$, density $\rho_0 = 7700\,\mathrm{kg/m^3}$, relative permittivity $\varepsilon_r = 700(1 - \mathrm{i}\tan\delta)$, dielectric loss $\tan\delta = 0.003$, piezo constant $h_{33} = 2.37 \times 10^9(1 + \mathrm{i}[1/(2Q_\mathrm{m}) + \tan\delta/2])\,\mathrm{V/m}$, and driving voltage 10 Vpp. The optimization is conducted for the half-wave resonance in the water layer and the objective is to obtain the maximum radiation force on a particle (spherical polystyrene bead with radius $a = 5\,\mu\mathrm{m}$, density $\rho_p = 1055\,\mathrm{kg/m^3}$, and bulk modulus $K = 4.061\,\mathrm{GPa}$) according to eqn (9a)-(9d).

A discussion with the authors revealed that the force magnitudes presented in the paper of Glynne-Jones et al.[6] are underestimated by up to 13% due to a minor error in the piezoelectric loss implementation. However, this has no impact on the trends that were presented and only little impact on the optimum configurations that were identified. In their paper, the optimization is visualized by cut planes through the parameter space. Two layer thicknesses are iterated in a gridwise manner, the remaining two are kept constant, the frequency is tuned to the half-wave resonance and the radiation force maximum within the fluid layer is plotted. For verification purposes, Glynne-Jones et al. provided their simulation code to the authors and Fig. 6(a) of their paper was reproduced with the corrected loss implementation as shown in Fig. 3(a). Here, the maximum radiation force is plotted over the fluid layer ($0.27\,\mathrm{mm} \le l_\mathrm{f} \le 0.50\,\mathrm{mm}$) and the reflector thickness ($0.04\,\mathrm{mm} \le l_\mathrm{r} \le 1.40\,\mathrm{mm}$) while keeping the carrier layer thickness at $l_\mathrm{c} = 0\,\mu\mathrm{m}$. At a frequency of 1.908 MHz, the global radiation force maximum of 294 pN appears with $l_\mathrm{f} = 0.36\,\mathrm{mm}$ and $l_\mathrm{r} = 0.74\,\mathrm{mm}$. The obtained frequency is different from the theoretical half-wave resonance frequency (2.06 MHz) under the assumption of hard walls at top and bottom of the fluid layer. The difference can be explained by the interaction of the individual device layers. Each layer defines the boundary conditions for neighboring layers, leading

to a combination of transmission and reflection at each material interface. In this sense, it is rather a device resonance with a strong field in the fluid than a pure fluid resonance (which does not exist for compliant boundaries) that leads to the strongest acoustic field.

For the automated optimization, the FE model is set up as a 2D simulation in order to be able to use a predefined module for the piezoelectric layer whereas symmetry is enforced to ensure a 1D characteristic. The reflector, the carrier and the fluid layer are modeled as acoustic domains with the same parameters as stated above. The tensors that describe the piezoelectric constitutive law are taken from Ferroperm[40] since PZT4D is equivalent to PZ26. The loss is accounted for by complex stiffness, permittivity, and stress piezoelectric coefficient tensors,

$$c^E_{\lambda\mu} = c'^E_{\lambda\mu} + \mathrm{i}\, c'^E_{\lambda\mu}/Q_\mathrm{m}, \tag{18a}$$
$$\varepsilon^S_{ik} = \varepsilon'^S_{ik} - \mathrm{i}\,\varepsilon'^S_{ik} \tan\delta, \tag{18b}$$
$$e_{i\mu} = e'_{i\mu} + \mathrm{i}\, e'_{i\mu}(1/(2Q_\mathrm{m}) - \tan\delta/2), \tag{18c}$$

where $c'^E_{\lambda\mu}$, ε'^S_{ik}, and $e'_{i\mu}$ are the real-valued parameters provided by Ferroperm. During the optimization, the geometry is successively remeshed according to the updated device geometry. The mesh settings need to be chosen such that sufficient resolution is ensured for all parameter combination. Here, we choose rectangular elements of quadratic order with a maximal element size of 5 µm and automatic refinement for very thin layers. In order to check the simulation results, the cut plane which is defined above is generated using the FE model instead and shown in Fig. 3(b). The plotted radiation force maxima match remarkably well with a relative error of less than 1%.

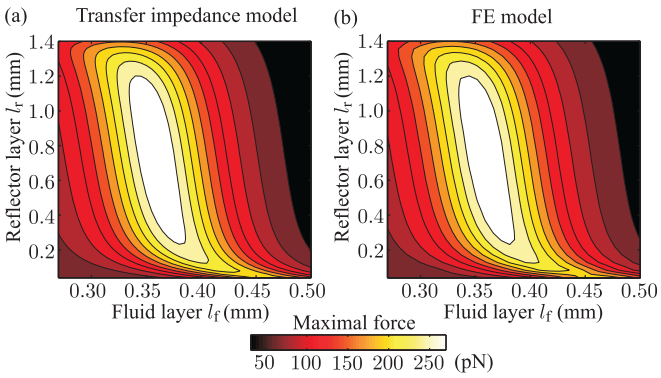

Fig. 3 Maximum radiation force on a 10 µm polystyrene bead in a planar resonator working at the half-wave resonance. The results are plotted over varying reflector and the fluid layer thickness as obtained with a 1 mm piezoelectric layer and zero carrier layer. In (a), the device model of Glynne-Jones et al. is used whereas (b) shows the results of the FE model.

With the optimum configuration in mind, the FE model of the planar resonator is optimized as a proof of concept. This optimization is performed over the whole parameter space,

$$1\,\mathrm{MHz} \le f \le 3\,\mathrm{MHz}, \tag{19a}$$
$$0\,\mathrm{mm} \le l_\mathrm{c} \le 1.40\,\mathrm{mm}, \tag{19b}$$
$$0.27\,\mathrm{mm} \le l_\mathrm{f} \le 0.50\,\mathrm{mm}, \tag{19c}$$
$$0.04\,\mathrm{mm} \le l_\mathrm{r} \le 1.40\,\mathrm{mm}, \tag{19d}$$

with the objective to obtain a maximum radiation force magnitude on a polystyrene bead, as described above. The resonance frequency of the transducer is affected by both its thickness and the boundary conditions to the top and bottom of the transducer material. Therefore, the desired transducer resonance frequency which leads to strong excitation is affected by the other device materials as well as the other layer thicknesses. This uncertainty is taken care of by exploring a relatively large frequency range. To comply with the minimizing convention of the optimization problem, the objective function is the negative radiation force magnitude within the fluid layer. The GA settings are chosen as specified in section 3.4 with arelatively small population size of 100 individuals to account for the relatively small number of local optima in the parameter space. The crossover fraction is set to 0.5 and all parameters are normalized with their upper limit in order to achieve equal weighting in the optimization. As shown in Fig. 4, the best objective function value obtained in each generation is plotted over a total of 150 generations. Also shown is the mean objective function

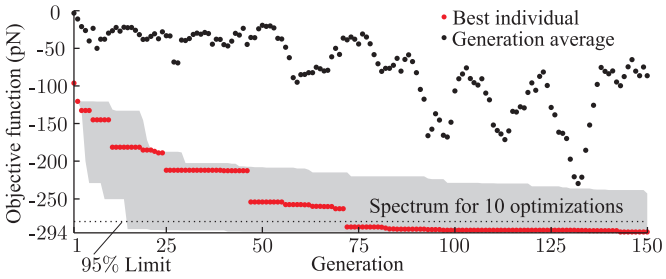

Fig. 4 Convergence of a planar resonator optimization. The objective function corresponding to the best individual in each generation and the average objective function are plotted over 150 GA-generations. The objective function is defined as the negative radiation force magnitude in the fluid and the population size is 100 individuals. For ten repetitions of the optimization, the spectrum of best individuals is visualized as a gray area.

in each generation. The optimization result found after 11.2 hours of computation with four parallel threads is a radiation force of 294 pN and a pressure magnitude of 1.08 MPa at a frequency of 1.910 MHz with $l_\mathrm{c} = 0$ mm, $l_\mathrm{f} = 0.35$ mm, and $l_\mathrm{r} = 0.94$ mm. This result is very close to what is expected given the analysis of Glynne-Jones et al. and it indicates that the optimization code is working properly. Nevertheless, it is important to be aware that there is never a guarantee that the global optimum is found after a certain time. The optimization is repeated

ten times to analyze the convergence and the spectrum of best results obtained in each generation. From Fig. 4 it becomes apparent that the initial generation in the Matlab GA implementation is chosen randomly but repeatably if no constraints have to be fulfilled. During the first 50 generations, all optimizations converge fast to radiation forces above 200 pN. After 120 generations, eight out of ten optimizations are within 5% of the global optimum. The fastest optimization reaches this level already after 15 generations.

4.2 Optimization of a 3D Micro-Device

Here, we demonstrate that device design by optimization is also applicable to 3D micro-devices. As an example, a device for the positioning of hollow glass particles, similar to the one used by Leibacher et al. is chosen.[48] It is a typical micro-device with a silicon layer containing the etched fluid chamber and channels, a glass lid that is bonded on top of the silicon and a piezoelectric element that is glued to the bottom of the device. The geometry of the assembled device is shown in Fig. 5. The piezoelectric material is modeled with the constitutive equations eqn (18a)-(18c), the material parameters are adopted from section 4.1 and the polarization is in z-direction. The elastic properties of monocrystalline silicon are taken from the literature[38] for a (100)-wafer with the x- and y-axis of the device in $\langle 110 \rangle$ crystal directions. Damping is neglected for silicon. Glass is modeled as linear elastic isotropic solid of density $\rho = 2240\,\mathrm{kg/m^3}$, having the Lamé storage parameters $\lambda' = 23.1\,\mathrm{GPa}$ and $\mu' = 24.1\,\mathrm{GPa}$.[37] Due to the lack of exact Lamé loss parameters, they are approximated from the attenuation of 2 dB/m for irrotational ultrasound waves at 1 MHz.[49] The equivalent Lamé loss parameters are then $\lambda'' = 9.6\,\mathrm{MPa}$ and $\mu'' = 10.0\,\mathrm{MPa}$. Water is modeled as an acoustic domain with $c_0 = 1480\,\mathrm{m/s}$ and $\rho_0 = 1000\,\mathrm{kg/m^3}$. An FE analysis that includes the damping due to the viscous boundary layer has been used to determine the loss factor of $\varphi = 0.004$ for the desired mode in the fluid chamber. The thin layer of conductive epoxy glue (EPO-TEK H20E) between the transducer and the silicon is modeled with a thin layer approximation to keep the computational effort at a reasonable level. The glue has the Lamé parameters $\lambda' = 3.22\,\mathrm{GPa}$, $\mu' = 2.14\,\mathrm{GPa}$, $\lambda'' = 322\,\mathrm{MPa}$, $\mu'' = 214\,\mathrm{MPa}$ and a layer thickness of 20 µm.[50] For simplicity, the piezoelectric element is driven at 5 Vpp in the simulation. However, if heat is the limiting factor in an experimental setup, it is reasonable to alter the driving conditions to constant power dissipation. In case the anchor losses can be neglected, all energy in the device is eventually dissipated into heat, which is why the total power dissipation is equal to the power consumption of the piezoelectric element. This power consumption is calculated easily in an FE analysis and the acoustic field variables scale linearly with the actuation amplitude. Therefore, constant power dissipation can be enforced easily for all frequencies and parameter combinations. The governing equations and fluid-structure interaction are implemented as described in section 2.1. Radiation into surrounding materials is neglected since it is assumed that the device is surrounded by air and placed on foam. For this reason, the stress free boundary condition is applied everywhere on the device surface. The FE analysis solves for approximately 300000 degrees of freedom using a relatively fine mesh (around 20 elements per wavelength in water) that consists of around 70000 tetrahedral elements of quadratic order. One simulation run takes around 72 seconds. Of course, the successive remeshing due to the changed geometry changes these numbers. Care must be taken in the choice of the meshing settings to ensure that the mesh quality is not compromised by unfortunate parameter combinations.

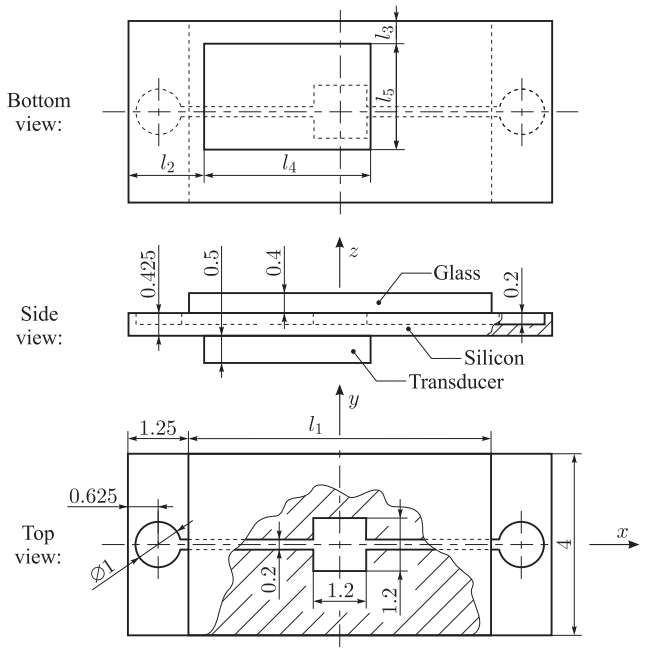

Fig. 5 Geometry of the 3D acoustofluidic micro-device for the positioning of hollow particles in a square fluidic chamber. The five geometric parameters (l_1 to l_5) that are varied by the optimization algorithm define the length of the middle section as well as the size and position of the piezoelectric transducer.

Hollow glass particles with a radius of 9.95 µm and the scattering coefficients $f_1 = 0.602$ and $f_2 = -0.362$ in water can be positioned in the center of the square fluid cavity if the so-called (1,1)-mode with the pressure field,

$$p = \hat{p}\sin(\pi x/l_{\mathrm{fc}})\sin(\pi y/l_{\mathrm{fc}}), \qquad (20)$$

is excited.[48] Herein, $\hat{p}$ is the magnitude of the pressure field and the coordinates x and y are centered in the square cavity of side-length $l_{\mathrm{fc}} = 1.2\,\mathrm{mm}$. The normalized absolute pressure field in the fluid cavity is visualized in Fig. 6(a). The corresponding force potential is calculated by inserting eqn (20) and (5) into the Gor'kov potential eqn (9a)-(9d). The result is the reference force potential for the optimization since optimal positioning of particles

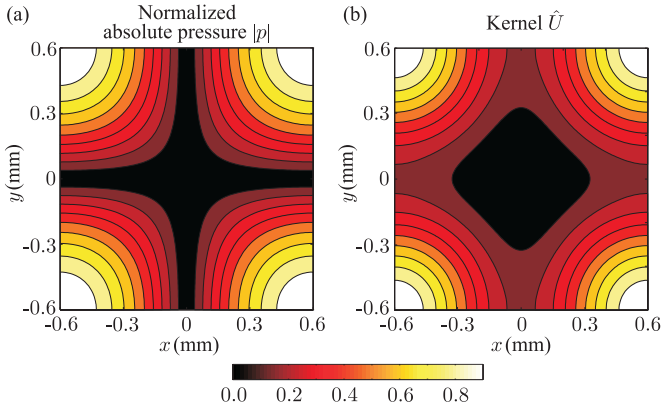

Fig. 6 The normalized absolute pressure field $|p|$ and the kernel $\hat{U}$ of the objective function are plotted in (a) and (b), respectively. They are both calculated based on the theoretically optimal pressure field eqn (20). The particles gather at the minimum of the kernel function in the center of the chamber.

in the center of the cavity is expected at this mode. As shown in Fig. 6(b), the kernel $\hat{U}$ for the objective function eqn (17) is therefore obtained through normalization of the calculated Gor'kov potential. Theoretically, not only eigenmodes but any arbitrarily function could be chosen as kernel and the optimization would still lead to a force potential that fits as good as possible. However, if the FE analysis is a frequency domain simulation of a single frequency, the range of attainable shapes is rather limited because the wavelength is prescribed. It is important to be aware that the boundary conditions at the fluid cavity need to be suitable for the desired mode. This means, the device topology has to be chosen properly beforehand since it defines *e.g.* what kind of materials are bounding the fluid at which position. In the presented example, the cavity walls have a higher acoustic impedance than water, allowing pressure peaks to form at the boundaries. Furthermore, the inlet and outlet channels are located at the pressure minimum of the desired acoustic field to reduce the pressure amplitudes at the locations where it is not needed. In this way, the acoustic energy is focused in the square cavity, leading to high amplitudes.

The set of optimization parameters is chosen with the objective to minimize the size of the parameter space, yet retaining all important degrees of freedom for the optimization. As specified in Fig. 5, the geometric parameters include the size and the position of the piezoelectric element as well as the length of the middle device section. Symmetry is used to reduce the parameter ranges, *i.e.* in the bottom view of Fig. 5, the position of the upper left transducer corner can be limited to the upper left quarter of the device area without loss of generality. The excitation frequency is another optimization parameter. Assuming a perfectly rigid and square cavity, the (1,1)-mode appears at a frequency of 0.872 MHz.[48] In the FE simulation of the device, the desired mode develops at a similar frequency. In summary, the optimization parameter space is,

$$0.8\,\text{MHz} \le f \le 0.9\,\text{MHz}, \tag{21a}$$
$$3.0\,\text{mm} \le l_1 \le 6.0\,\text{mm}, \tag{21b}$$
$$0\,\text{mm} \le l_2 \le 4.0\,\text{mm}, \tag{21c}$$
$$0\,\text{mm} \le l_3 \le 1.5\,\text{mm}, \tag{21d}$$
$$1.0\,\text{mm} \le l_4 \le 8.5\,\text{mm}, \tag{21e}$$
$$1.0\,\text{mm} \le l_5 \le 4.0\,\text{mm}, \tag{21f}$$

whereas the inequality constraints,

$$l_2 + l_4 - l_1 \le 2.5\,\text{mm}, \tag{22a}$$
$$l_3 + l_5 \le 4\,\text{mm}, \tag{22b}$$

enforce that the piezoelectric element does not protrude over the edges of the silicon layer. The GA optimization is set up as specified in section 3.4 with a population size of 100 individuals and a crossover fraction of 0.5. All parameters are normalized with their upper limit in order to achieve equal weighting in the optimization. As shown in Fig. 7, the best objective function value obtained in each generation is plotted alongside with the average value of the objective function over a total of 40 generations which took 42 hours to compute using four parallel threads. The

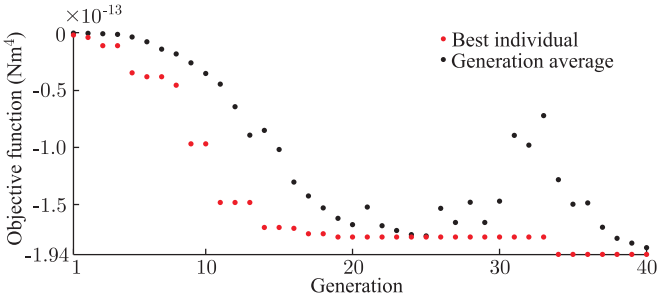

Fig. 7 Convergence of a 3D micro-device optimization. The objective function corresponding to the best individual in each generation and the average objective function are plotted over 40 GA-generations. The objective function is based on the Gor'kov potential as defined in eqn (17).

optimization converges fast and reaches the best objective function value of $-1.94 \times 10^{-13}\,\text{Nm}^4$ after 40 generations. The parameters corresponding to this best device design are $f = 0.840\,\text{MHz}$, $l_1 = 3.59\,\text{mm}$, $l_2 = 0.635\,\text{mm}$, $l_3 = 0.125\,\text{mm}$, $l_4 = 2.80\,\text{mm}$, and $l_5 = 2.51\,\text{mm}$. The obtained absolute pressure field with a magnitude of 2.63 MPa and the corresponding Gor'kov potential are shown in Fig. 8. In relation to measured pressure amplitudes of up to 2.4 MPa,[51] the optimization delivers an exceptionally strong acoustic field and by a comparison with Fig. 6, it becomes evident that the optimization produces the desired mode shape. This means, the optimization setup is able to design a device that is tailored for the specific application defined by the objective function.

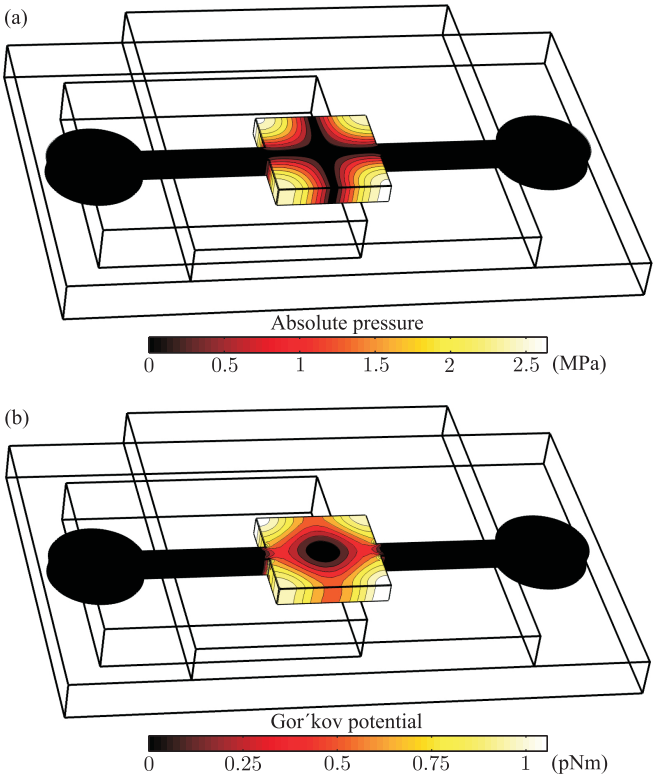

Fig. 8 Optimized device geometry. The obtained absolute pressure field and the Gor'kov force potential for the hollow glass particles are plotted in (a) and (b), respectively. The maximum force on the hollow particles reaches 1.2 nN.

5 Conclusion

The design process of acoustofluidic micro-devices increasingly relies on numerical simulations in order to achieve good device performance. However, finding a suitable geometry manually is very time consuming and often leaves a large margin for improvements. We have demonstrated that devices can be developed in an automatic fashion using numerical optimization. We emphasize that the full picture of all relevant physical phenomena, the numerical modeling, and the optimization process must be understood in order to implement a successful device design setup. We have given an overview of the numerical modeling of acoustofluidic micro-devices with a focus on the damping mechanisms which crucially affect the attainable radiation force magnitudes. These damping effects are difficult to implement accurately due to their complexity and the lack of precise material loss information. Details of our design by optimization implementation have been provided.† Our setup has been tested successfully with a planar resonator and converged to the established optimal geometry. Illustrating the practicability of the presented approach, a typical 3D micro-device for the manipulation of a specific particle type has been designed for optimal positioning capabilities at a predefined location. Even though the GA optimization works well and robustly, there is a potential to reduce the computational effort through hybrid approaches that combine stochastic and deterministic optimization.[11]

The main result of work is a numerical setup that can automatically design acoustofluidic devices. Compared to the repeated iteration of design and experiments or the manual optimization of numerical device models, our approach can save time and results in device designs of superior acoustophoretic performance. As the field of acoustofluidics is moving towards commercial lab-on-a-chip applications, optimal device performance becomes increasingly important whereas our automatic design by optimization approach is a flexible and powerful method to achieve this goal in a time-efficient manner.

References

1 H. Bruus, J. Dual, J. Hawkes, M. Hill, T. Laurell, J. Nilsson, S. Radel, S. Sadhal and M. Wiklund, *Lab Chip*, 2011, **11**, 3579–3580.
2 L. P. Gor'kov, *Sov. Phy. Dok. (Engl. Transl.)*, 1962, **6**, 773–775.
3 H. Bruus, *Lab Chip*, 2012, **12**, 1014–1021.
4 M. P. Bendsoe, in *Topology Optimization*, Springer, Berlin, 2003, pp. 1–2.
5 J. Svennebring, O. Manneberg, P. Skafte-Pedersen, H. Bruus and M. Wiklund, *Biotechnol. Bioeng.*, 2009, **103**, 323–328.
6 P. Glynne-Jones, R. J. Boltryk and M. Hill, *Lab Chip*, 2012, **12**, 1417–1426.
7 J. Nocedal and S. J. Wright, *Numerical Optimization*, Springer, New York, 1999.
8 G. Kress and D. Keller, *Structural Optimization*, ETH Zurich lecture notes, 2007.
9 P. Venkataraman, *Applied Optimization with MATLAB Programming*, Wiley, New Jersey, 2nd edn, 2009.
10 J. C. Spall, *Introduction to Stochastic Search and Optimization*, Wiley, New Jersey, 2003.
11 K. R. Deibel and K. Wegener, *JMSY*, 2013, **32**, 523–528.
12 L. Chen and D. Wang, *JMSA*, 2007, **6**, 55–61.
13 H. Bruus, *Lab Chip*, 2011, **11**, 3742–3751.
14 J. Dual and T. Schwarz, *Lab Chip*, 2012, **12**, 244–252.
15 J. Dual and D. Moller, *Lab Chip*, 2012, **12**, 506–514.
16 H. Bruus, *Lab Chip*, 2012, **12**, 20–28.
17 M. Settnes and H. Bruus, *Phys. Rev. E*, 2012, **85**, 016327.
18 H. Bruus, *Lab Chip*, 2012, **12**, 1578–1586.
20 P. Glynne-Jones, P. P. Mishra, R. J. Boltryk and M. Hill, *J. Acoust. Soc. Am.*, 2013, **133**, 1885–1893.
19 J. Dual, P. Hahn, I. Leibacher, D. Moller, T. Schwarz and J. Wang, *Lab Chip*, 2012, **12**, 4010–4021.
21 P. Hahn, T. Baasch and J. Dual, Proc. of Acoustofluidics Conf., Southampton, UK, 2013, pp. 28–29.

22 M. Weiser, R. Apfel and E. Neppiras, *Acta Acustica u.w. Acustica*, 1984, **56**, 114–119.

23 R. Górecki, M. Mars, W. Alda, L. Fioretti and J. Rybicki, *Task Quaterly*, 2001, **5**, 59–69.

24 N. Riley, *Ann. Rev. Fluid Mech.*, 2001, **33**, 43–65.

25 S. S. Sadhal, *Lab Chip*, 2012, **12**, 2292–2300.

26 M. Wiklund, R. Green and M. Ohlin, *Lab Chip*, 2012, **12**, 2438–2451.

27 R. Barnkob, P. Augustsson, T. Laurell and H. Bruus, Proc. of μTAS 2010, Groningen, The Netherlands, 2010, pp. 1247–1249.

28 P. B. Muller, R. Barnkob, M. J. H. Jensen and H. Bruus, *Lab Chip*, 2012, **12**, 4617–4627.

29 W. L. Nyborg, *J. Acoust. Soc. Am.*, 1953, **25**, 68–75.

30 J. Lei, M. Hill and P. Glynne-Jones, *Lab on a Chip*, 2014, **14**, 532–541.

31 L. E. Kinsler, A. R. Frey, A. B. Coppens and J. V. Sanders, *Fundamentals of Acoustics*, Wiley, New York, 2nd edn, 2000.

32 R. M. Christensen, *Theory of Viscoelasticity*, Academic Press, New York, 2nd edn, 1982.

33 J. T. Karlsen, M. W. H. Ley, P. B. Muller and H. Bruus, Proc. of Acoustofluidics Conf., Southampton, UK, 2013, pp. 67–68.

34 W. M. Haynes, D. R. Lide and T. J. Bruno, *CRC Handbook of Chemistry and Physics 2012-2013*, CRC press, Boca Raton, FL, 93rd edn, 2012.

35 J. M. Carcione, *Wave Fields in Real Media*, Elsevier, Oxford, 2nd edn, 2007.

36 C. T. Leondes, *Structural Dynamic Systems Computational Techniques and Optimization: Computational Techniques*, CRC Press, 1999, vol. 7.

37 A. R. Selfridge, *IEEE Trans. Sonics Ultrason.*, 1985, **32**, 381–394.

38 M. A. Hopcroft, W. D. Nix and T. W. Kenny, *JMEMS*, 2010, **19**, 229–238.

39 B. Kim, M. A. Hopcroft, R. N. Candler, C. M. Jha, M. Agarwal, R. Melamud, S. A. Chandorkar, G. Yama and T. W. Kenny, *JMEMS*, 2008, **17**, 755–766.

40 *Ferroperm webpage*, `http://www.ferroperm-piezo.com/`.

41 K. Uchino and S. Hirose, *Trans. Ultrason., Ferroelectr., Freq. Control*, 2001, **48**, 307–321.

42 S. Sherrit and B. K. Mukherjee, *ArXiv e-prints arXiv:0711.2657*, 2007.

43 H. Campanella, *Acoustic Wave and Electromechanical Resonators: Concept to Key Applications*, Artech House, Norwood, MA, 2010.

44 U. Basu and A. K. Chopra, *Computer Methods in Applied Mechanics and Engineering*, 2003, **192**, 1337 – 1375.

45 B. Harrington and R. Abdolvand, *J. Micromech. Microeng.*, 2011, **21**, 085021.

46 M. Gröschl, *Acustica*, 1998, **84**, 432–447.

47 J. Reddy, *An Introduction to the Finite Element Method*, McGraw-Hill, 3rd edn, 2005.

48 I. Leibacher, W. Dietze, P. Hahn, J. Wang, S. Schmitt and J. Dual, *Microfl. Nanofl.*, 2013, 1–12.

49 L. Mordfin, *Handbook of Reference Data for Nondestructive Testing*, ASTM, West Conshohocken, PA, 2002.

50 *EPO-TEK webpage*, `http://www.epotek.com/`.

51 R. Barnkob, P. Augustsson, T. Laurell and H. Bruus, *Lab Chip*, 2010, **10**, 563–570.

Graphical abstract

Design by optimization reduces the development time of new acoustofluidic micro-devices and maximizes their acoustophoretic performance.